

Research Paper

Label-Free Luminescent Mesoporous Silica Nanoparticles for Imaging and Drug Delivery

Hongmin Chen^{1*}, Zipeng Zhen^{1*}, Wei Tang¹, Trevor Todd¹, Yen-Jun Chuang², Lianchun Wang³, Zhengwei Pan², and Jin Xie¹✉

1. Department of Chemistry and Bio-Imaging Research Center (BIRC), University of Georgia, Athens, GA 30602, United States;
2. Faculty of Engineering, University of Georgia, Athens, GA 30602, United States;
3. Department of Biochemistry and Complex Carbohydrate Research Center (CCRC), University of Georgia, Athens, GA 30602, United States.

* These authors contributed equally to this work.

✉ Corresponding author: E-mail: jinxie@uga.edu.

© Ivyspring International Publisher. This is an open-access article distributed under the terms of the Creative Commons License (<http://creativecommons.org/licenses/by-nc-nd/3.0/>). Reproduction is permitted for personal, noncommercial use, provided that the article is in whole, unmodified, and properly cited.

Received: 2013.05.11; Accepted: 2013.05.22; Published: 2013.08.10

Abstract

We report herein a straightforward and label-free approach to prepare luminescent mesoporous silica nanoparticles. We found that calcination at 400 °C can grant mesoporous organosilica nanoparticles with strong fluorescence of great photo- and chemical stability. The luminescence is found to originate from the carbon dots generated from the calcination, rather than the defects in the silica matrix as was believed previously. The calcination does not impact the particles' abilities to load drugs and conjugate to biomolecules. In a proof-of-concept study, we demonstrated that doxorubicin (Dox) can be efficiently encapsulated into these fluorescent mesoporous silica nanoparticles. After coupled to c(RGDyK), the nanoconjugates can efficiently home to tumors through interactions with integrin $\alpha_v\beta_3$ overexpressed on the tumor vasculature. This calcination-induced luminescence is expected to find wide applications in silica-based drug delivery, nanoparticle coating, and immunofluorescence imaging.

Key words: Silica nanoparticles; Drug delivery; Integrin $\alpha_v\beta_3$; Bioimaging; Doxorubicin.

Introduction

Mesoporous silica nanoparticles, due to their low toxicity and high loading capacity, have been widely used as a drug delivery vehicle [1-3]. Small molecule drugs, such as doxorubicin (Dox) and camptothecin, have been loaded onto mesoporous silica nanoparticles and studied for cancer treatment [4-7]. Mesoporous silica has also been widely used as a coating material [8, 9]. Nanoparticles made from a pyrolysis method, for instance, can be coated with a layer of silica and granted with good stability in aqueous solutions [3, 10-20]. Both applications can benefit from the facile surface chemistry of silica that allows easy coupling of targeting ligands onto the particles [6].

To facilitate the tracking of silica or silica-coated nanoparticles in a biological system, it is common to label silica particles with a fluorophore. This can be an organic dye molecule, which is loaded through either physical adsorption or chemical conjugation; alternatively, a nanoparticle fluorophore—for instance a quantum dot [21] or a upconversion nanoparticle [22, 23]—can be used, in which case the particles are encapsulated by a silica shell. These fluorophore-doping methods however, can be time-consuming and expensive, and are commonly associated with issues like high toxicity, increased particle size, and dye-leaking [21, 24, 25].

We report herein that a simple calcination at 400 °C can grant mesoporous silica nanoparticles luminescence (**Scheme 1/Figure A**). The mild treatment does not cause changes to the particles' size, shape, pore size, stability, and loading capacity. The resulting fluorescent mesoporous silica (FL-SiO₂) nanoparticles possess strong fluorescence that is stable against photo-bleaching and environmental changes. The luminescence, interestingly, was found attributed to small carbon dots generated from the calcination (**Scheme 1/Figure A**). We demonstrated that these label-free silica fluorophores can be tracked both *in vitro* and *in vivo*, suggesting the great potential of this technology in drug delivery, nanoparticle coating, and immunofluorescence imaging.

Results

We first prepared 3-aminopropyl triethoxy silane (APTES)-containing mesoporous silica particles [26], and subjected the products to calcination at 400 °C for 2 h. **Figure 1a** and **1b** are TEM images of 80 nm mesoporous silica nanoparticles before and after calcination, respectively. The treatment caused no nanoparticle aggregation and little change to the particles' appearances. The resulting FL-SiO₂ nanoparticles retained their ordered mesoporous structures with a pore size of about 3 nm (**Figure 1c**) [27, 28].

While untreated mesoporous silica nanoparticles are transparent, FL-SiO₂ nanoparticles displayed a broad absorption spectrum with a shoulder at ca. 360 nm (**Figure 1d**). When excited in the range of 320-360

nm, FL-SiO₂ nanoparticles exhibited strong fluorescence (**Figure 1d**). **Figure 1e** is a photograph of FL-SiO₂ nanoparticles in a powder and solution under excitation at 365 nm. Strong blue luminescence was visualized even by the naked eye. Increasing the excitation wavelength resulted in a red-shift of the emission; the shift, however, was at a cost of the luminescence intensity (**Figure 1d**). For instance, when excited at 460 nm, the emission peak was shifted to 520 nm, and the maximum intensity was ~50% of that excited at 380 nm. The same treatment also works for mesoporous nanoparticles of different sizes and even solid silica nanoparticles (Supplementary Material: **Figure S1**).

For conventional organic fluorophores, two primary drawbacks are the poor photostability and chemical stability. **Figure 1f** (red spots) shows that the emission intensity of Texas Red (a commonly used dye molecule, ex/em: 589/615 nm) dropped rapidly after exposure to excitation light, and was completely bleached within 120 s [29]. In contrast, FL-SiO₂ nanoparticles exhibited no drop in fluorescent intensity under continual illumination for 10 min (**Figure 1f**, blue dots). In fact, we found no change of fluorescence intensity even after 24 h of UV irradiation (data not shown). The luminescence was also stable against environmental changes, as we found a constant fluorescence intensity at different pH (from 4 to 9) and in a strong reducing environment (100 mM dithiothreitol, or DTT) (**Figure 1g**).

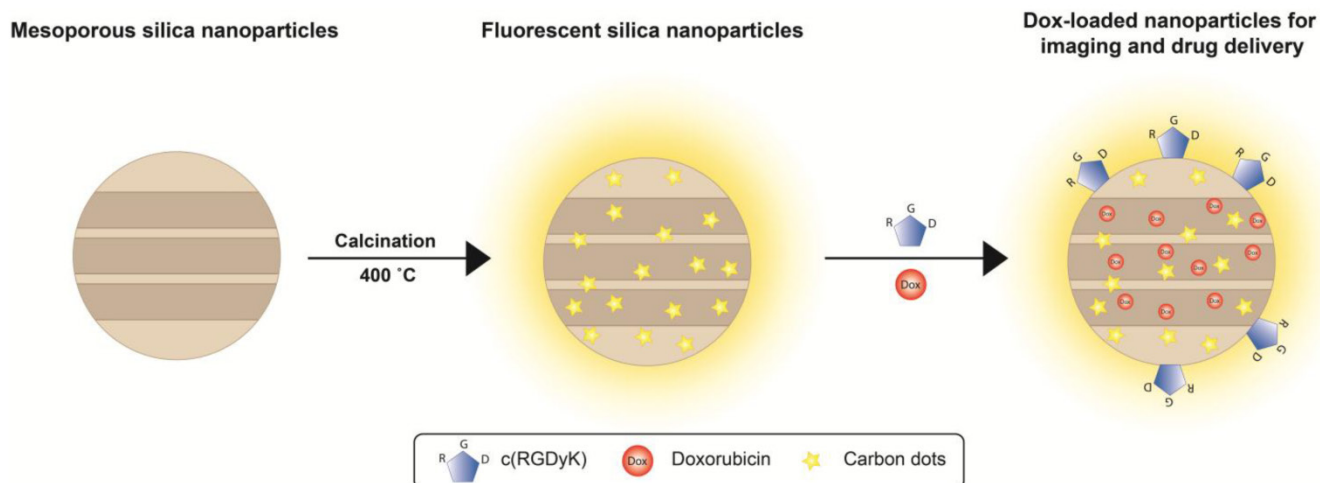


Figure A. (Scheme 1). Schematic illustration of the particle formation and drug loading. After being calcinated at 400 °C, mesoporous organosilica nanoparticles are rendered fluorescent due to the generation of carbon dots in the matrix. These fluorescent silica nanoparticles can be loaded with drug molecules (e.g. Dox) and coupled with targeting motifs (e.g. RGD peptide) for simultaneous imaging and drug delivery.

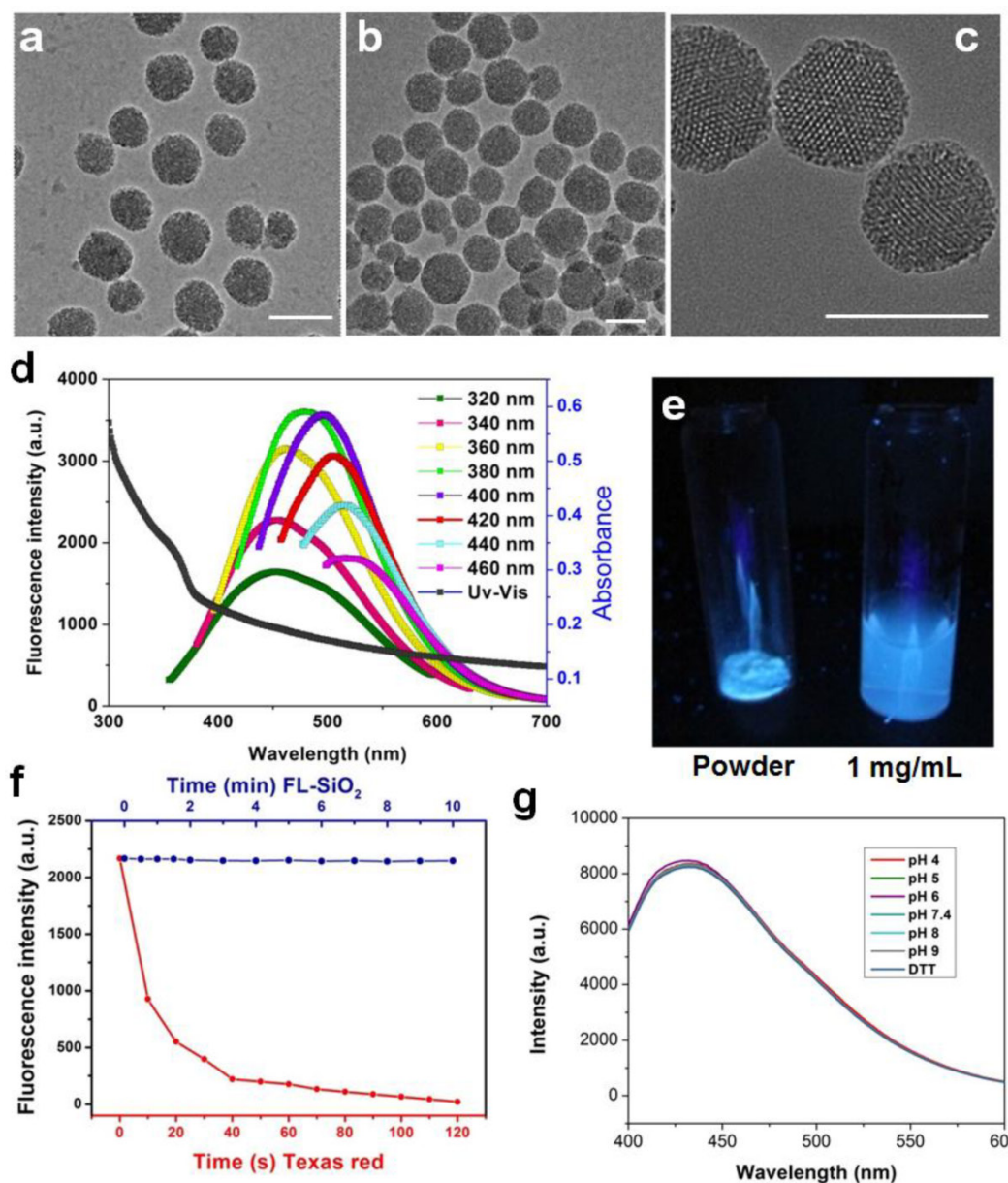


Fig 1. TEM images of mesoporous silica nanoparticles before (a) and after (b&c) calcination. No obvious morphology change was observed. Scale bars: 100 nm. d) Absorption and emission spectra of FL-SiO₂ nanoparticles. The fluorescence intensity was at the maximum when the particles were excited at ~380 nm. e) FL-SiO₂ nanoparticles in powder and solution under excitation at 365 nm. f) Photostability of Texas Red (red dots) and FL-SiO₂ nanoparticles (blue dots). When exposed to excitation light, Texas Red was quickly bleached. FL-SiO₂ nanoparticles, on the other hand, showed robust photostability. g) The fluorescence intensities of FL-SiO₂ nanoparticles remained constant at different pH (from 4 to 9), and in a highly reducing environment. The incubation was carried out at room temperature for 24 h.

We next examined the impact of calcination on the particles' biocompatibility and drug loading efficiency. The cytotoxicity studies were performed with U87MG human glioblastoma cells by MTT assays, which found no toxicity of FL-SiO₂ nanoparticles in the tested concentration range (0-100 µg/mL) (**Figure 2a**). Drug loading was studied with 80 nm FL-SiO₂ nanoparticles using Dox as a model drug. After overnight incubation, we observed a high loading rate of ~70 wt% (i.e. ~ 0.7 g Dox/g FL-SiO₂). This number is similar to what was reported previously with com-

mon mesoporous SiO₂ nanoparticles [4-6, 26, 30], suggesting that the calcination causes no pore clogging. The loaded Dox can be gradually released (**Figure 2b**) [31]. When studied in a PBS buffer (pH 7.4), we found a cumulative release rate of ~20% in 50 h, which is also similar to the previous reports [32, 33]. When tested with U87MG cells, these Dox-loaded FL-SiO₂ nanoparticles induced a concentration dependent viability drop (**Figure 2a**).

For bio-conjugation purposes, we coated FL-SiO₂ nanoparticles with APTES. The resulting, aminated

FL-SiO₂ (NH₂-FL-SiO₂) nanoparticles were covalently coupled with c(RGDyK), which has a high affinity toward integrin $\alpha_v\beta_3$, a tumor biomarker overexpressed on tumor vasculature and tumor cells of various types [34-38]. The coupling had little impact on the particles' stability (Supplementary Material: **Figure S2**) and Dox loading rate (remained at 70 wt%). When incubated with U87MG cells, which overexpress $\alpha_v\beta_3$ on the surface, the RGD-conjugated FL-SiO₂ (RGD-FL-SiO₂) were efficiently internalized (**Figure 2c**). NH₂-FL-SiO₂ nanoparticles, on the other hand, showed little cellular uptake under the same conditions.

In vivo imaging studies were performed on U87MG subcutaneous tumor models. 0.14 mg of RGD-FL-SiO₂ nanoparticles were intravenously (i.v.) injected (n = 3), and fluorescence images were acquired on a Maestro II scanner at different time points. We found good accumulation of fluorescence activities in the tumors at 4 and 24 h (**Figure 3a**). In addition to the tumors, activities were also found in the liver and backbone, which were attributed to particle uptake by the Kupffer cells in the liver and macrophages in the bone marrow, respectively [39, 40]. In the control group, NH₂-FL-SiO₂ nanoparticles at the same dose were injected (n = 3). Despite a certain degree of tumor accumulation, the intensity in the tumors was significantly lower than that in the RGD-FL-SiO₂ group. After the 24 h imaging, the animals were sacrificed. The tumors as well as major

organs were harvested for *ex vivo* imaging. The distribution pattern is similar to the *in vivo* results except a high level of activities in the intestine is seen (**Figure 3a**). The signals from intestine however, showed a spectrum that is different from that of RGD-FL-SiO₂ nanoparticles (Supplementary Material: **Figure S3**). These signals were due to digested food, not the particles [31, 41, 42]. The relatively low intensity in the liver and spleen is attributed to the strong tissue absorption. The luminescence is the most intense in the region of 400-550 nm where body tissue is less transparent than in the NIR spectrum window.

We also studied the potential of FL-SiO₂ nanoparticles in histology. In a separate study, we injected Dox loaded RGD-FL-SiO₂ (Dox-RGD-FL-SiO₂) nanoparticles into U87MG tumor models (5 mg Dox/kg mice, n = 3). In the control group, Dox loaded NH₂-FL-SiO₂ nanoparticles (Dox-FL-SiO₂) at the same dose were injected. We sacrificed the animals after 24 h, and performed histology studies with the tumor sections. In the Dox-RGD-FL-SiO₂ group, we observed strong fluorescence from both silica and Dox. The signals were well correlated (**Figure 3b**), and clearly delineated the shape of blood vessels, suggesting that most of the Dox-RGD-FL-SiO₂ nanoparticles were retained within the blood vessels, presumably through interactions with integrin $\alpha_v\beta_3$ expressed on the tumor vasculature [43, 44]. This concept was supported by results from the control group, where few signals from either Dox or silica were observed.

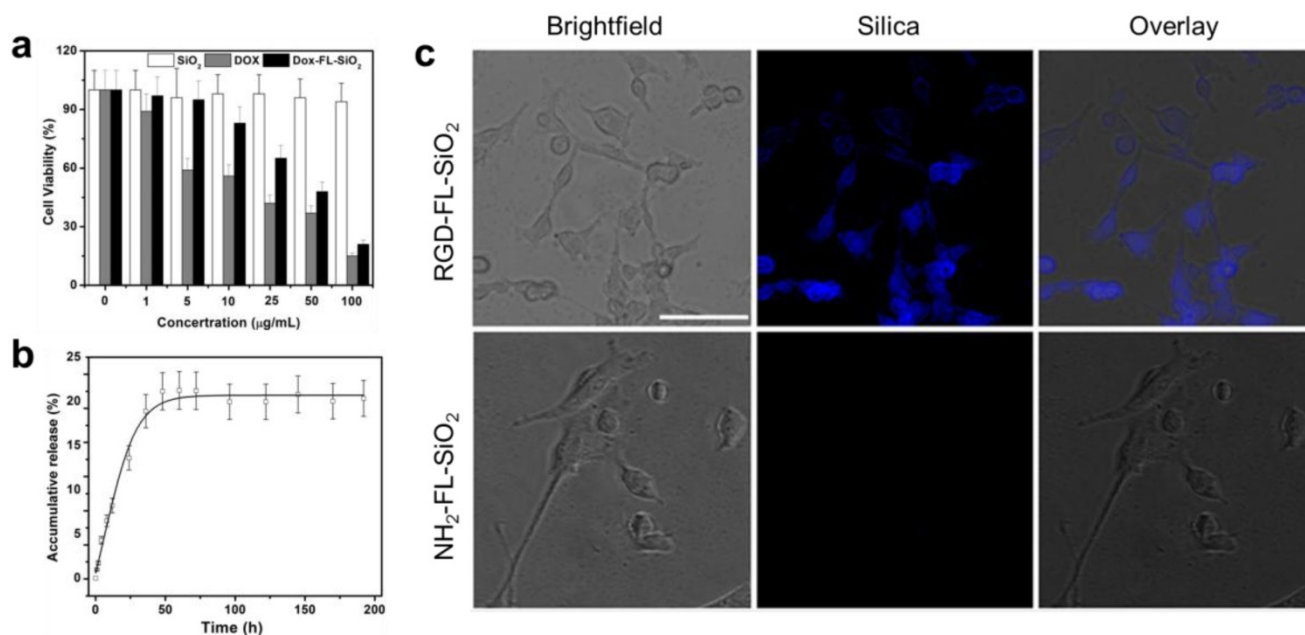


Fig 2. a) Cytotoxicity studies. FL-SiO₂ nanoparticles were not toxic to U87MG cells in the tested concentration range (0-100 $\mu\text{g/mL}$). On the other hand, Dox-FL-SiO₂ nanoparticles showed concentration dependent toxicity against U87MG cells. b) Drug release study with Dox-FL-SiO₂ nanoparticles in PBS. c) Cellular uptake studies. After being incubated with U87MG cells for 1 h, we observed good uptake with RGD-FL-SiO₂ nanoparticles, but not with NH₂-FL-SiO₂ nanoparticles. The fluorescence signals are from the FL-SiO₂ nanoparticles. Scale bar: 50 μm .

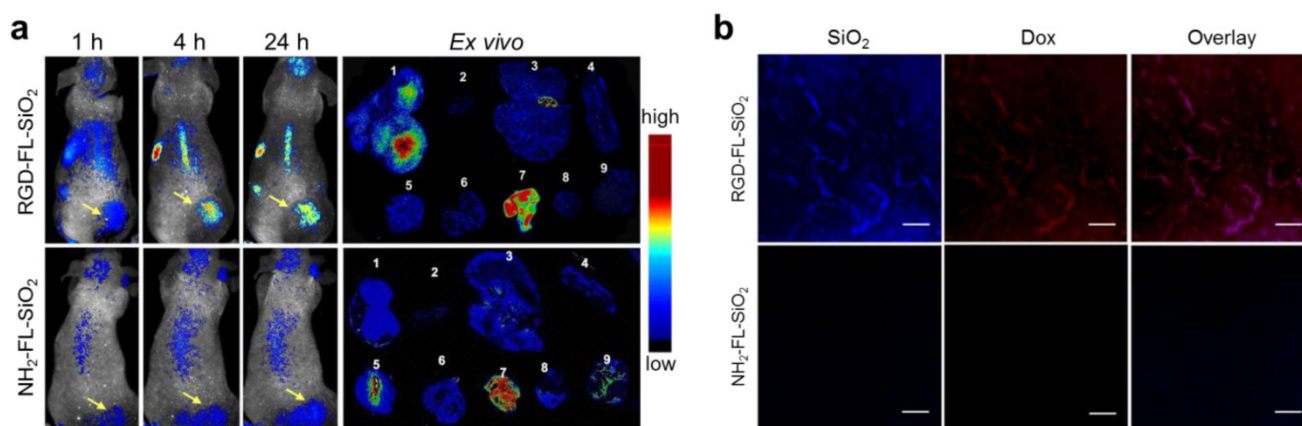


Fig 3. a) *In vivo* and *ex vivo* imaging results. RGD-FL-SiO₂ and NH₂-FL-SiO₂ nanoparticles were i.v. injected into U87MG tumor-bearing mice. The images were acquired at 1, 4 and 24 h post injection. After 24 h imaging, tumors and major organs were dissected and laid on a sheet of black paper for *ex vivo* imaging. The tissues were arranged by the following order: 1) tumor; 2) heart; 3) liver; 4) spleen; 5) lung; 6) kidneys; 7) intestine; 8) muscle; 9) brain. b) Microscopic fluorescence imaging studies with tumor sections that were taken from U87MG tumor-bearing mice injected with either Dox-RGD-FL-SiO₂ or Dox-NH₂-FL-SiO₂ nanoparticles. Scale bars: 50 μm.

Discussion and conclusions

Incorporating an organic functional group into the silica matrix, in this case amine (from APTES), is essential to the generation of luminescence. For mesoporous SiO₂ nanoparticles made from pure TEOS, the calcination failed to render the particles fluorescent. The functional group, however, is not limited to amine. When a thiol-containing silane (e.g. 3-mercaptopropyltrimethoxysilane) was used as a precursor, the resulting SiO₂ nanoparticles, after calcination, also showed strong luminescence (Supplementary Material: **Figure S1g&1h**). The luminescence is dependent on the calcination temperature. Calcination at 210 °C resulted in nanoparticles with moderate emission intensity (Supplementary Material: **Figure S4 & S5**), whereas calcination at a high temperature (600 °C) resulted in much weaker fluorescence (Supplementary Material: **Figure S5**).

Similar calcination-induced luminescence was observed by the Tan and Schmedake groups with solid silica nanoparticles [45, 46], and by Sailor *et al.* with silica sol-gels [47]. To our knowledge, however, there have been no reports on calcination-induced fluorescence of mesoporous silica nanoparticles, and no investigations on the potential of the fluorescence in bioimaging. In all the previous studies, the fluorescence was attributed to the defects in the silica matrix [45, 47]. Briefly, calcination-induced decomposition creates a C substitutional defect for Si, which is believed to be a luminescent species [47]. To test the theory, we incubated FL-SiO₂ nanoparticles with hydrofluoric acid (HF, 37%) to decompose the silica matrix. Surprisingly, the resulting solution remained fluorescent with an almost unchanged intensity, suggesting that the previous hypothesis is untrue (**Figure 4a&b**). Further TEM studies with the HF-treated FL-SiO₂ solution confirmed the complete destruction

of the silica matrix (**Figure 4c**). Instead, we found many ca. 3 nm carbon dots (C-Dots) in the remaining solution (**Figure 4c**), which we believe are the true luminescence source. Indeed, previous studies with C-Dots showed a luminescence spectrum that is similar to ours [48-50]. It is noted, however, that synthesis of C-Dots was mostly achieved through harsh chemical synthesis and required post-synthesis surface passivation to be rendered strong fluorescence [51]. Our discovery suggests an alternative and milder synthetic approach for C-Dot preparation. Though not the direct source, the defects in the silica skeleton are critical to the generation of C-Dots, as calcination is unable to illuminate pure silica particles (data not shown). It is possible that these defects serve as the originating sites where C-Dots begin to grow. The porous silica structure is also believed to be essential, providing small nanoreactors for particle formation and preventing overgrowth. Further investigations on the formation of C-Dots and their differences from those made by the previous methods are ongoing.

Aside from rendering nanoparticles fluorescent, the calcination does not affect the particles' other characteristics, such as the size, shape, pore size, and biocompatibility. The resulting nanoparticles can be treated as uncalcined ones in terms of loading drugs and conjugation with biomolecules. In this study, we showed that Dox can be loaded onto FL-SiO₂ nanoparticles with high efficiency. We expect that other small molecule-based drugs can be loaded *via* a similar mechanism. Different peptide sequences, as well as antibodies and aptamers, should also be able to be tethered onto the particle surface [52-54]. Integrin specific cytotoxicity and *in vivo* treatment were not studied with Dox-RGD-FL-SiO₂ nanoparticles. But due to comparable drug loading and release, we expect that the therapeutic profiles are similar to the

uncalcinated ones.

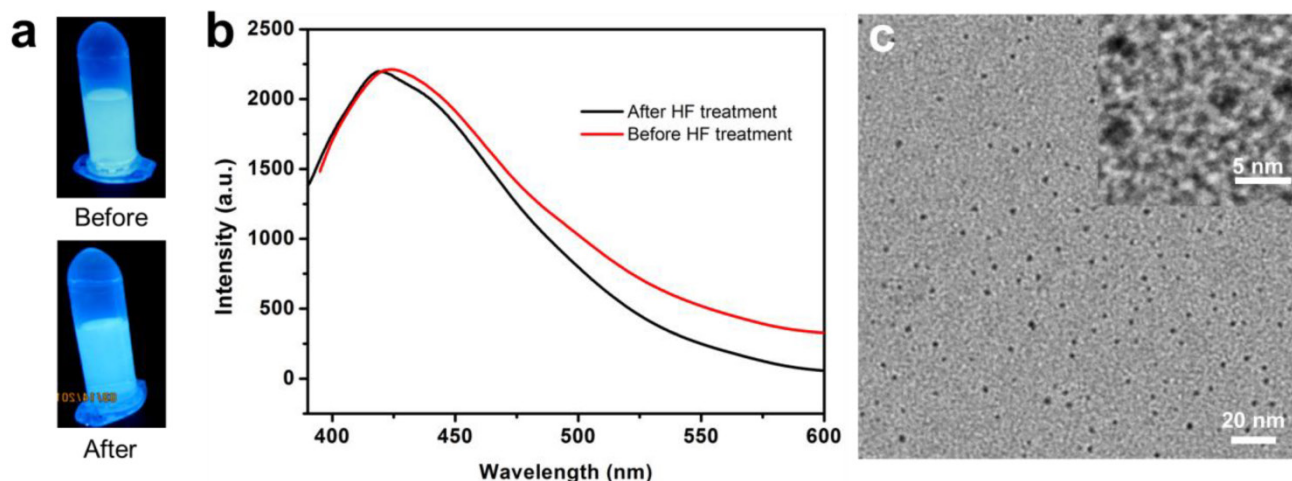


Fig 4. a) Photographs taken before and after incubation of FL-SiO₂ nanoparticle with HF. The solution remained luminescent after the treatment. b) Emission spectra of FL-SiO₂ nanoparticles, taken before and after HF treatment. c) TEM image of FL-SiO₂ nanoparticles after being treated with HF. Silica matrix was removed, leaving C-Dots with a diameter of ~3 nm.

FL-SiO₂ nanoparticles show exceptional photo-stability, exhibiting constant fluorescence even after hours of UV irradiation. The fluorescence was also proved stable against environmental changes, no matter at high/low pH or in a strong reducing environment (**Figure 1g**). This quality is important because chemical surroundings change drastically across cell membranes, and among different cellular organelles. For instance, glutathione (GSH), a thiol-containing reducing molecule, is at a level of 70 mM inside tumor cells, which is ~7 times higher than that in the circulation [55, 56]. And while pH stays neutral in most cell organelles, it drops to as low as 4.5 in endosomes/lysosomes [57, 58]. The chemical- and photo-stability ensures constant and enduring fluorescence output, which is critical for quantitative analyses.

The emission of FL-SiO₂ nanoparticles is the most intense in the visible spectrum region. Such a short emission wavelength may limit their uses in *in vivo* imaging, as a high level of tissue autofluorescence may intervene. On the other hand, autofluorescence is less a concern in a histology setting. As demonstrated, the fluorescence of FL-SiO₂ nanoparticles can benefit immunofluorescence investigations. And since FL-SiO₂ nanoparticles are extremely stable in an acidic environment, it is also possible to harness the fluorescence for accurate biodistribution analysis.

Overall, we developed a straightforward and label-free method to grant mesoporous silica nanoparticles with strong and stable fluorescence. We identified the calcination-induced C-Dots, rather than the defects in the silica matrix, as the true source of luminescence. These findings are expected to have extensive and profound impact considering the wide

use of silica in drug delivery and particle coating.

Methods and materials

Synthesis and characterizations of FL-SiO₂ nanoparticle: Mesoporous silica nanoparticles were prepared following a previously published procedure [26]. Briefly, 0.2 g cetyltrimethylammonium bromide (CTAB) was dissolved in 96 mL water. With magnetic stirring, 0.7 mL of 2 M sodium hydroxide (NaOH) was added, and the resulting solution was heated up to 80 °C. Subsequently, 1.4 mL tetraethyl orthosilicate (TEOS), 3 mL ethylacetate, and desired amounts of organosilanes, (e.g. APTES, N-[3-(trimethoxysilyl)propyl]ethylenediamine, or 3-mercaptopropyltrimethoxysilane), were added, and the mixture was stirred at 80 °C for 2 h. The raw product was collected by centrifugation, washed 3 times with ethanol, and re-dispersed in ethanol. To remove CTAB, 40 μL saturated HCl was added to the particle suspension and the solution was stirred for 3 h at 60 °C. The particles were washed twice with ethanol, and dried at 60 °C overnight. The powders were first treated at low temperatures (< 200 °C), and then calcined in a muffle furnace at 400 °C for 2 h in the open air. The resulting particles were functionalized by APTES in dry toluene to obtain amine-functionalized FL-SiO₂ (NH₂-FL-SiO₂) nanoparticles. Transmission electron microscopy (TEM) was carried out on a FEI Tecnai20 transmission electron microscope operating at 200 kV accelerating voltage. Fluorescence spectra were recorded on a Hitachi F-7000 fluorescence spectrophotometer. UV-Vis absorbance spectra were measured on a BioTek Synergy MX multi-mode microplate reader. Hydrodynamic size distribution was measured by dynamic light scattering (DLS) on a Malvern Zeta Nanosizer.

RGD conjugation: NH₂-FL-SiO₂ nanoparticles were dispersed in PBS buffer (pH = 7.4). Into the solution, bis(sulfosuccinimidyl) suberate (BS3) (100×) in DMSO was added. After incubation at room temperature for 30 min, the activated particles were collected by centrifugation, washed 3 times with PBS, and redispersed in PBS. c(RGDyK) (200×) in DMSO was added to the activated NH₂-FL-SiO₂ solution, and the mixture was incubated at room temperature for 2 h. The resulting RGD conjugated FL-SiO₂ (RGD-FL-SiO₂) nanoparticles were collected by centrifugation, washed, and redispersed in PBS (pH = 7.4).

Dox loading and release: NH₂-FL-SiO₂ or RGD-FL-SiO₂ nanoparticles (1 mg/mL, 1 mL) and Dox (2 mg/mL, 0.5 mL) were mixed in PBS, and the solution was stirred overnight at room temperature. The products, Dox-loaded NH₂-FL-SiO₂ or RGD-FL-SiO₂ nanoparticles (Dox-NH₂-FL-SiO₂ and Dox-RGD-FL-SiO₂), were collected by centrifugation. The supernatant was collected for UV-Vis spectroscopic studies to determine the amount of Dox that was loaded. The drug release studies were performed at room temperature with a slide-A-lyzer dialysis device (10K MWCO, Pierce). Dox-NH₂-FL-SiO₂ and Dox-RGD-FL-SiO₂ nanoparticles were loaded onto the device, and the device was immersed in 15 mL PBS (pH 7.4). At selective time points, 1 mL solution was taken from the tube and replaced with 1 mL fresh PBS. The Dox concentrations in the sample solutions were measured by fluorescence spectrometry and compared to a standard curve. Experiments were performed in triplicates.

In vitro cell uptake: U87MG human glioblastoma cells were cultured in MEM supplemented with 2 mM L-glutamine, 1.5 g/L sodium bicarbonate, 0.1 mM nonessential amino acids, 1.0 mM sodium pyruvate, and 10% fetal bovine serum at 37°C in a humidified atmosphere with 5% CO₂. To study the cellular uptake, 10⁵ U87MG cells were seeded onto each well of a 4-chamber slide (Lab-Tek) one day prior to the studies. Briefly, RGD-FL-SiO₂ nanoparticles were added into the chambers to reach a final concentration of 25 µg/mL. In the control group, NH₂-FL-SiO₂ nanoparticles of the same amount were added. The incubation was stopped after 1 h, and the cells were rinsed 3 times with PBS (pH 7.4). The slides were mounted and imaged under an Olympus X71 fluorescence microscope. The cell viability was assessed by MTT assays using a gradient of Dox-RGD-FL-SiO₂ nanoparticles (Dox concentrations of 1, 5, 10, 25, 50 and 100 µg/mL). For controls, free Dox and NH₂-FL-SiO₂ nanoparticles were studied.

Animal models: Animal studies were performed according to a protocol approved by the Institutional

Animal Care and Use Committee (IACUC) of University of Georgia. The U87MG tumor models were generated by subcutaneously injecting 5 × 10⁶ cells in 100 µL PBS into the right hindlimb of 4-6 week athymic nude mice (Harlan).

In vivo imaging studies: The imaging studies were performed on U87MG tumor-bearing mice when the tumors reached a size between 200 and 500 mm³. RGD-FL-SiO₂ and NH₂-FL-SiO₂ nanoparticles at the same amount (7.1 mg/kg) were intravenously injected (n = 3). Whole body fluorescence images were acquired on a Maestro II imaging system (PerkinElmer) at 1, 4, and 24 h post injection using a 500-720 nm emission filter with exposure time of 0.3 sec. After the 24 h imaging, the animals were sacrificed. Tumors as well as major organs were harvested and subjected to *ex vivo* imaging. To evaluate FL-SiO₂ nanoparticles in *in vivo* tracking, Dox-RGD-FL-SiO₂ or Dox-NH₂-FL-SiO₂ at 5 mg Dox/kg were intravenously injected (n = 3). Animals were sacrificed after 24 h, and the tumors were collected, snap-frozen, and sectioned into 10 µm slices. Images were taken on an Olympus IX71 fluorescence microscope and analyzed by a software provided by the vendor.

Supplementary Material

Fig.S1 – S5. <http://www.thno.org/v03p0650s1.pdf>

Acknowledgements

This work was supported by NIH grants 5R00CA153772 (J.X.) and RR005351/GM103390 (L.W.). T.T. was supported by a Philbrook scholarship. We thank Mackenzie Walls for the cover and illustration work.

Competing Interests

The authors have declared that no competing interest exists.

References

1. Xie J, Liu G, Eden HS, Ai H, Chen X. Surface-engineered magnetic nanoparticle platforms for cancer imaging and therapy. *Acc Chem Res.* 2011; 44: 883-92.
2. Xie J, Lee S, Chen X. Nanoparticle-based theranostic agents. *Adv Drug Deliv Rev.* 2010; 62: 1064-79.
3. Lin X, Xie J, Niu G, Zhang F, Gao H, Yang M, et al. Chimeric ferritin nanocages for multiple function loading and multimodal imaging. *Nano Lett.* 2011; 11: 814-9.
4. Muhammad F, Guo M, Qi W, Sun F, Wang A, Guo Y, et al. pH-Triggered controlled drug release from mesoporous silica nanoparticles via intracellular dissolution of ZnO nanolids. *J Am Chem Soc.* 2011; 133: 8778-81.
5. Liu H, Chen D, Li L, Liu T, Tan L, Wu X, et al. Multifunctional gold nanoshells on silica nanorattles: a platform for the combination of photothermal therapy and chemotherapy with low systemic toxicity. *Angew Chem Int Ed Engl.* 2011; 50: 891-5.
6. Ashley CE, Carnes EC, Phillips GK, Padilla D, Durfee PN, Brown PA, et al. The targeted delivery of multicomponent cargos to cancer cells by nanoporous particle-supported lipid bilayers. *Nat Mater.* 2011; 10: 389-97.
7. Lu J, Liong M, Zink JJ, Tamanoi F. Mesoporous silica nanoparticles as a delivery system for hydrophobic anticancer drugs. *Small.* 2007; 3: 1341-6.

8. Erathodiyil N, Ying JY. Functionalization of inorganic nanoparticles for bioimaging applications. *Acc Chem Res.* 2011; 44: 925-35.
9. Guerrero-Martinez A, Perez-Juste J, Liz-Marzan LM. Recent progress on silica coating of nanoparticles and related nanomaterials. *Adv Mater.* 2010; 22: 1182-95.
10. Xie J, Zhang F, Aronova M, Zhu L, Lin X, Quan Q, et al. Manipulating the power of an additional phase: a flower-like Au-Fe₃O₄ optical nanosensor for imaging protease expressions in vivo. *ACS Nano.* 2011; 5: 3043-51.
11. Mikhaylov G, Mikac U, Magaeva AA, Itin VI, Naiden EP, Psakhye I, et al. Ferri-liposomes as an MRI-visible drug-delivery system for targeting tumours and their microenvironment. *Nat Nanotech.* 2011; 6: 594-602.
12. Fan K, Cao C, Pan Y, Lu D, Yang D, Feng J, et al. Magnetoferritin nanoparticles for targeting and visualizing tumour tissues. *Nat Nanotech.* 2012; 7: 833.
13. Lin X, Xie J, Zhu L, Lee S, Niu G, Ma Y, et al. Hybrid Ferritin Nanoparticles as Activatable Probes for Tumor Imaging. *Angew Chem Int Ed Engl.* 2011; 50: 1569-72.
14. Valero E, Tambalo S, Marzola P, Ortega-Munoz M, Lopez-Jaramillo FJ, Santoyo-Gonzalez F, et al. Magnetic nanoparticles--templated assembly of protein subunits: a new platform for carbohydrate-based MRI nanoprob. *J Am Chem Soc.* 2011; 133: 4889-95.
15. Zrazhevskiy P, Sena M, Gao X. Designing multifunctional quantum dots for bioimaging, detection, and drug delivery. *Chem Soc Rev.* 2010; 39: 4326-54.
16. Bagalkot V, Gao X. siRNA-aptamer chimeras on nanoparticles: preserving targeting functionality for effective gene silencing. *ACS Nano.* 2011; 5: 8131-9.
17. Park JH, Gu L, von Maltzahn G, Ruoslahti E, Bhatia SN, Sailor MJ. Biodegradable luminescent porous silicon nanoparticles for in vivo applications. *Nat Mater.* 2009; 8: 331-6.
18. Ang LY, Lim ME, Ong LC, Zhang Y. Applications of upconversion nanoparticles in imaging, detection and therapy. *Nanomedicine (Lond).* 2011; 6: 1273-88.
19. Yavuz MS, Cheng Y, Chen J, Cogley CM, Zhang Q, Rycenga M, et al. Gold nanocages covered by smart polymers for controlled release with near-infrared light. *Nat Mater.* 2009; 8: 935-9.
20. Benachour H, Seve A, Bastogne T, Frochot C, Vanderesse R, Jasniewski J, et al. Multifunctional Peptide-conjugated hybrid silica nanoparticles for photodynamic therapy and MRI. *Theranostics.* 2012; 2: 889-904.
21. Hu X, Gao X. Silica-polymer dual layer-encapsulated quantum dots with remarkable stability. *ACS Nano.* 2010; 4: 6080-6.
22. Idris NM, Gnanasammandhan MK, Zhang J, Ho PC, Mahendran R, Zhang Y. In vivo photodynamic therapy using upconversion nanoparticles as remote-controlled nanotransducers. *Nat Med.* 2012; 18: 1580-U190.
23. Qian HS, Guo HC, Ho PCL, Mahendran R, Zhang Y. Mesoporous-Silica-Coated Up-Conversion Fluorescent Nanoparticles for Photodynamic Therapy. *Small.* 2009; 5: 2285-90.
24. Auger A, Samuel J, Poncelet O, Raccourt O. A comparative study of non-covalent encapsulation methods for organic dyes into silica nanoparticles. *Nanoscale Res Lett.* 2011; 6(1):328.
25. Wang L, Wang KM, Santra S, Zhao XJ, Hilliard LR, Smith JE, et al. Watching silica nanoparticles glow in the biological world. *Anal Chem.* 2006; 78: 646-54.
26. Kim J, Kim HS, Lee N, Kim T, Kim H, Yu T, et al. Multifunctional uniform nanoparticles composed of a magnetite nanocrystal core and a mesoporous silica shell for magnetic resonance and fluorescence imaging and for drug delivery. *Angew Chem Int Ed Engl.* 2008; 47: 8438-41.
27. Chen H, He J. Fine control over the morphology and structure of mesoporous silica nanomaterials by a dual-templating approach. *Chem Commun.* 2008; 4422-4.
28. Gu J, Fan W, Shimoyama A, Okubo T. Organic-inorganic mesoporous nanocarriers integrated with biogenic ligands. *Small.* 2007; 3: 1740-4.
29. Gao X, Yang L, Petros JA, Marshall FF, Simons JW, Nie S. In vivo molecular and cellular imaging with quantum dots. *Curr Opin Biotechnol.* 2005; 16: 63-72.
30. Gao Y, Chen Y, Ji X, He X, Yin Q, Zhang Z, et al. Controlled intracellular release of doxorubicin in multidrug-resistant cancer cells by tuning the shell-pore sizes of mesoporous silica nanoparticles. *ACS Nano.* 2011; 5: 9788-98.
31. Troy T, Jekic-McMullen D, Sambucetti L, Rice B. Quantitative comparison of the sensitivity of detection of fluorescent and bioluminescent reporters in animal models. *Mol Imaging.* 2004; 3: 9-23.
32. Li L, Tang F, Liu H, Liu T, Hao N, Chen D, et al. In vivo delivery of silica nanorattle encapsulated docetaxel for liver cancer therapy with low toxicity and high efficacy. *ACS Nano.* 2010; 4: 6874-82.
33. Gao F, Li L, Liu T, Hao N, Liu H, Tan L, et al. Doxorubicin loaded silica nanorattles actively seek tumors with improved anti-tumor effects. *Nanoscale.* 2012; 4: 3365-72.
34. Ye Y, Chen X. Integrin targeting for tumor optical imaging. *Theranostics.* 2011; 1: 102-26.
35. Chen K, Chen X. Integrin targeted delivery of chemotherapeutics. *Theranostics.* 2011; 1: 189-200.
36. Cai W, Shin DW, Chen K, Gheysens O, Cao Q, Wang SX, et al. Peptide-labeled near-infrared quantum dots for imaging tumor vasculature in living subjects. *Nano Lett.* 2006; 6: 669-76.
37. Li Y, Li Z, Wang X, Liu F, Cheng Y, Zhang B, et al. In vivo cancer targeting and imaging-guided surgery with near infrared-emitting quantum dot bioconjugates. *Theranostics.* 2012; 2: 769-76.
38. Guo W, Chen N, Tu Y, Dong C, Zhang B, Hu C, et al. Synthesis of Zn-Cu-In-S/ZnS core/shell quantum dots with inhibited blue-shift photoluminescence and applications for tumor targeted bioimaging. *Theranostics.* 2013; 3: 99-108.
39. Lunov O, Syrovets T, Loos C, Beil J, Delacher M, Tron K, et al. Differential uptake of functionalized polystyrene nanoparticles by human macrophages and a monocytic cell line. *ACS Nano.* 2011; 5: 1657-69.
40. Choi CH, Zuckerman JE, Webster P, Davis ME. Targeting kidney mesangium by nanoparticles of defined size. *Proc Natl Acad Sci U S A.* 2011; 108: 6656-61.
41. Inoue Y, Izawa K, Kiryu S, Tojo A, Ohtomo K. Diet and abdominal autofluorescence detected by in vivo fluorescence imaging of living mice. *Mol Imaging.* 2008; 7: 21-7.
42. Bhaumik S, DePuy J, Klimash J. Strategies to minimize background autofluorescence in live mice during noninvasive fluorescence optical imaging. *Lab Anim (NY).* 2007; 36: 40-3.
43. Chen X. Integrin Targeted Imaging and Therapy. *Theranostics.* 2011; 2011: 28-9.
44. Lim EH, Danthi N, Bednarski M, Li KC. A review: Integrin alphavbeta3-targeted molecular imaging and therapy in angiogenesis. *Nanomedicine (Lond).* 2005; 1: 110-4.
45. Wang L, Estevez MC, O'Donoghue M, Tan W. Fluorophore-free luminescent organosilica nanoparticles. *Langmuir.* 2008; 24: 1635-9.
46. Jakob AM, Schmedake TA. A novel approach to monodisperse, luminescent silica spheres. *Chem Mater.* 2006; 18: 3173-5.
47. Green WH, Le KP, Grey J, Au TT, Sailor MJ. White phosphors from a silicate-carboxylate sol-gel precursor that lack metal activator ions. *Science.* 1997; 276: 1826-8.
48. Anilkumar P, Cao L, Yu JJ, Tackett KN, 2nd, Wang P, Mezziani MJ, et al. Crosslinked carbon dots as ultra-bright fluorescence probes. *Small.* 2013; 9: 545-51.
49. Bourlinos AB, Stassinopoulos A, Anglos D, Zboril R, Karakassides M, Giannelis EP. Surface functionalized carbogenic quantum dots. *Small.* 2008; 4: 455-8.
50. Tao H, Yang K, Ma Z, Wan J, Zhang Y, Kang Z, et al. In Vivo NIR Fluorescence Imaging, Biodistribution, and Toxicology of Photoluminescent Carbon Dots Produced from Carbon Nanotubes and Graphite. *Small.* 2011.
51. Wang X, Cao L, Yang ST, Lu F, Mezziani MJ, Tian L, et al. Bandgap-like strong fluorescence in functionalized carbon nanoparticles. *Angew Chem Int Ed Engl.* 2010; 49: 5310-4.
52. Farokhzad OC, Cheng J, Teplý BA, Sherifi I, Jon S, Kantoff PW, et al. Targeted nanoparticle-aptamer bioconjugates for cancer chemotherapy in vivo. *Proc Natl Acad Sci U S A.* 2006; 103: 6315-20.
53. Liu Z, Cai W, He L, Nakayama N, Chen K, Sun X, et al. In vivo biodistribution and highly efficient tumour targeting of carbon nanotubes in mice. *Nat Nanotechnol.* 2007; 2: 47-52.
54. Li LY, Wartchow CA, Danthi SN, Shen ZM, Dechene N, Pease J, et al. A novel antiangiogenesis therapy using an integrin antagonist or anti-FLK-1 antibody coated Y-90-labeled nanoparticles. *Int J Radiat Oncol.* 2004; 58: 1215-27.
55. Liu J, Pang Y, Huang W, Huang X, Meng L, Zhu X, et al. Bioreducible micelles self-assembled from amphiphilic hyperbranched multiarm copolymer for glutathione-mediated intracellular drug delivery. *Biomacromolecules.* 2011; 12: 1567-77.
56. Russo A, DeGraff W, Friedman N, Mitchell JB. Selective modulation of glutathione levels in human normal versus tumor cells and subsequent differential response to chemotherapy drugs. *Cancer Res.* 1986; 46: 2845-8.
57. Sorkin A, Von Zastrow M. Signal transduction and endocytosis: close encounters of many kinds. *Nat Rev Mol Cell Biol.* 2002; 3: 600-14.
58. Huotari J, Helenius A. Endosome maturation. *EMBO J.* 2011; 30: 3481-500.